We are IntechOpen, the world's leading publisher of Open Access books Built by scientists, for scientists

6,900
Open access books available

185,000
International authors and editors

200M
Downloads

Our authors are among the

154
Countries delivered to

TOP 1%
most cited scientists

12.2%
Contributors from top 500 universities

WEB OF SCIENCE™

Selection of our books indexed in the Book Citation Index in Web of Science™ Core Collection (BKCI)

Interested in publishing with us?
Contact book.department@intechopen.com

Numbers displayed above are based on latest data collected.
For more information visit www.intechopen.com

9

The Controlled Growth of Long AlN Nanorods and *In Situ* Investigation on Their Field Emission Properties

Fei Liu*, Lifang Li, Zanjia Su, Shaozhi Deng, Jun Chen and Ningsheng Xu
GuangDong Province Key Laboratory of Display Material and Technology,
School of Physics and Engineering,
Sun Yat-sen University, Guangzhou,
People's Republic of China

1. Introduction

Wide bandgap semiconductor nanostructures have been the research focus in recent years because of their unique physical and chemical properties and low electron affinity, which benefits for tunnel emission (Geis et al., 1991; Zhirnov et al., 1997; Kang et al., 2001; Liu et al., 2009). Among them, AlN nanostructures should deserve paid much attention due to their high melting-point (> 2300 ^{o}C), high thermal conductivity (K ~ 320 W/m·k), large exciton binding energy and strong endurance to harsh environment (Davis, 1991; Nicolaescu et al., 1994; Sheppard et al., 1990; Ponthieu et al., 1991). There have emerged many synthesis methods to fabricate different morphology of AlN nanostructures, such as nanocone, nanorod, and nanorods (Liu et al., 2009; Zhao et al., 2004; Liu et al., 2004; Tang et al., 2005; Shi et al., 2005, 2006; Wu et al., 2003; Paul et al., 2008). But for actual device applications of AlN nanostructures, there still exist many technique questions, which need to be solved as soon as possible. Firstly, the controlled growth of large area AlN nanostructures with uniform morphology is very difficult because of which cares about the uniformity of their physical properties in devices. Secondly, systemic investigation on the field emission (FE) properties of AlN nanostructures is not enough, which has fallen behind the development of the preparing method. Thirdly, it is unknown to us all that what factors take effect on their FE behaviors and how to find optimal growth conditions for their device applications. So developing a suitable way to controllably prepare AlN nanostructures and investigate on their FE properties in detail is essential for promoting their progress in FE area.

Chemical vapor deposition (CVD) technique is an effective way to fabricate high density nanostructures with uniform morphology. Moreover, it has some merits in comparison with other ways, for example low-cost and easy to realize the controlled growth. By CVD technique, it is reported that different morphologies of AlN nanostructures (nanocones, nanorods, nanocraters and ultra-long nanorods) have been successfully fabricated on the substrate. Their formation mechanisms are respectively proposed for different morphology of nanostructures. In addition, their FE properties are investigated in detail.

* Corresponding Author

2. Experimental

Different mass ratios of Al powders (99.99 %) to Fe_2O_3 powders (99.99 %) were used as source materials. Fe_3O_4 nanoparticles were synthesized as the catalysts of the AlN nanocones, nanorods and nanocraters by high temperature solution phase reaction (Yang et al., 2003; He et al., 2001), which were spread over the substrate. The CVD system has been described in our recent works (Liu et al., 2004, 2005, 2008; Cao et al., 2003), as shown in Fig.1.

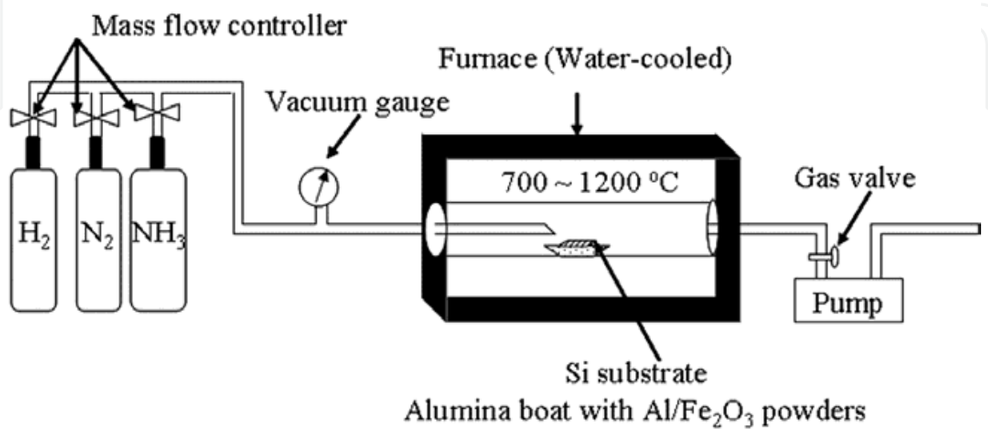

Fig. 1. A scheme of the chemical vapor deposition system in this experiment.

The reaction boat was put in the central region and the substrate was placed above the boat. A two-step increasing temperature method was used to synthesize AlN nanostructures. When the temperature arrived at 400 ℃, the reaction vessel was maintained here for 20 ~ 30 min in the carrier gas. In this step, the only difference between the growth of the nanorods and those of other nanostructures is that the carrier gas is H_2 instead of N_2. The base pressure of the chamber was better than 5 Pa, and the flow rate of N_2 or H_2 was kept at 200 sccm. When the temperature of central region was raised to the reaction temperature, and the mixed gas consisted of N_2 and NH_3 was introduced into the chamber. The flow rate ratio of N_2 to NH_3 was fixed at 200: 5 sccm ~ 200: 20 sccm and the reaction pressure was kept at 10 Torr in this procedure. The reaction temperature was ranging from 700 ◦C to 1200 ◦C and kept 1-8 hours for the synthesis of different morphologies of AlN nanostructures. When the chamber was cooled to room temperature, a grey white film was found on the substrate.

A field-emission type scanning electron microscope (XL-SFEG, FEI Corp.) was used to observe the morphologies of AlN nanostructures. Transmission electron microscopy (Tecnai-20, PHILIPS) and high-resolution transmission electron microscopy (Tecnai F20, FEI Corp.) were used to obtain the crystalline structure of the nanostructures, respectively. Field emission (FE) properties and work function of AlN nanostructures were performed on the Field emission analysis system and Omicron VT-AFM system equipped with ultraviolet photoelectron spectroscope (UPS), respectively.

3. Results and discussion

By adjusting the synthesis conditions, controlled growth of different morphologies of single-crystal AlN nanostructures has been successfully realized. XRD (X-ray diffraction) technique

was applied on four kinds of samples to confirm their chemical compositions. Typical XRD patterns of these four samples are provided in Fig. 2. It is found that there are four AlN characteristic peaks existing in these patterns, which correspond to the data of the Joint Committee for Powder Diffraction Standards (JCPDS) card No. 25-1133. Moreover, these four kinds of AlN nanostructures are found to be well-crystallized. It is also observed that Si (220) peak presenting in these patterns, which should come from the substrate. From these patterns, we can conclude that the alignment of all four samples is not very good because there still have other peaks than the growth direction of [001] existing in the patterns. Based on these patterns, it comes to a conclusion that all of the nanostructures in different morphology are AlN phase with a wurtzite structure.

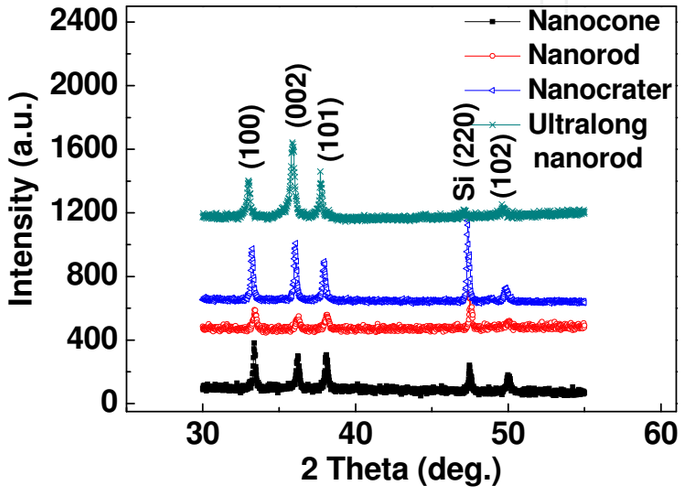

Fig. 2. Typical XRD patterns of AlN nanostructures with different morphologies.

The morphologies of four kinds of samples (nanocone, nanorod, nanocrater and ultra-long nanorod) are shown in Fig. 3. It is seen in Fig. 3a that the AlN nanocones have sharp tips and stand vertically to the substrate. From their high resolution SEM (scanning electron microscope) image (Fig. 3b), the nanocones are observed to have a length of about 2 μm and a mean radius at the top of 40 nm as well as they have smooth surface and high growth density. Fig. 3c shows the SEM image of AlN nanorod arrays in large area. These nanorods are perpendicular to the substrate and well-aligned. It is observed in Fig. 3d that the top of the nanorods seem to be well-facet hexagon and have uniform diameter. The length of the nanorods is about 2 micrometers and their averaged diameter is about 150 nanometers. The perspective view of AlN nanocrater arrays is provided in Fig. 3e. One can see that these AlN nanostructures grow perpendicularly to the silicon substrate and have uniform shapes. They are composed of many surrounded AlN nanocones with the same morphology and have crater-like shapes, so we denote them as nanocraters. In Fig. 3f they are seen have an outer diameter of 400 nm and a length of 2 μm. The top-view and side-view images of ultra-long AlN nanorod are respectively provided in Figs. 3g and 3h. The ultra-long nanorods are seen to have a mean diameter of 100 nm and an averaged length of 50 μm. Their diameter gradually decreases along their growth direction and lie to the substrate with an angle of 70^{o}. Among these four samples, it is obviously that the ultra-long AlN nanorod array has the highest aspect ratio (500) and the lowest growth density (3 $x10^{8}/cm^{2}$). Moreover, it is also

found that the AlN nanostructures are nearly in vertical arrays whether they are in what morphology, which will benefit for their FE applications.

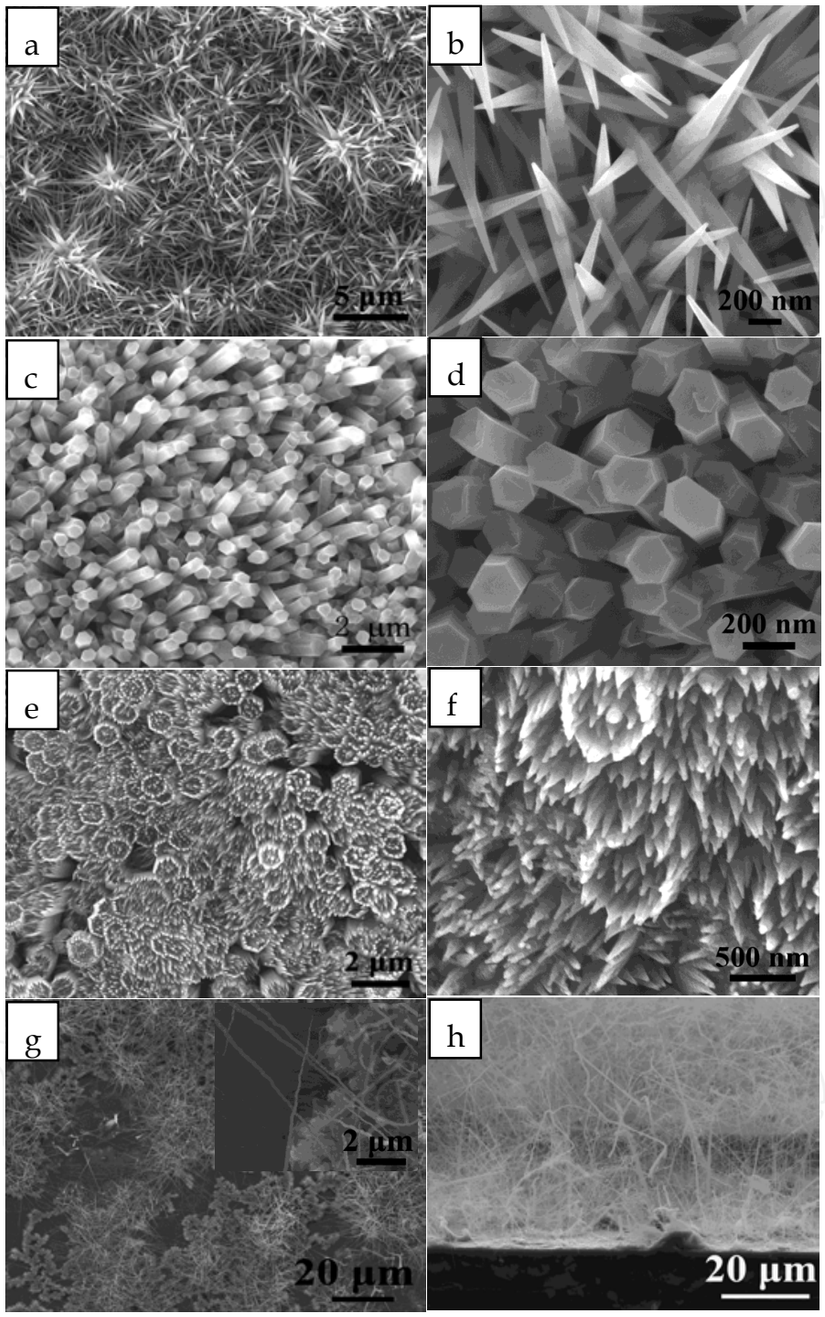

Fig. 3. (a, b) Low-resolution and high-resolution SEM images of the AlN nanocones, respectively. (c, d) Typical SEM images of the AlN nanorods in low magnification and high magnification, respectively. (e, f) The low magnification and high magnification images of the AlN nanocraters, respectively. (g, h) Top-view and side-view images of the ultra-long of nanorods.

To confirm the crystalline characteristics of AlN nanostructures in different morphology, TEM (transmission electron microscopy) technique was performed on these samples. Typical TEM image of AlN nanocone is shown in Fig. 4a. It is seen that the diameter of the nanocone is gradually decreasing from the bottom to the top, which is in agreement with our SEM results in Fig. 3a. The corresponding selected area electron diffraction (SAED) pattern is in the inset, in which one can see that the diffraction spots are clear and sharp. By identifying their clear diffraction spots, these nanocones are proved to have a perfect single crystalline AlN structure and have a growth direction of [001]. And the AlN nanorods have a uniform diameter through the whole length, as shown Fig. 4c. Further SAED (the inset) and HRTEM (Fig. 4d) characterizations indicate that they are also AlN single crystalline structures and grow along [001] direction, which is similar with the nanocones. Figs. 4e and 4f provide the general TEM image of AlN nanocraters, respectively. It is seen that the nanocrater is composed of several surrounded nanocones, as shown in Fig. 4e. Typical SAED pattern (the inset) and HRTEM image (Fig. 4f) of a nanocone (white ellipse) are provided to investigate their crystalline structures. It is noted that every nanocone appears the same diffraction spots and HRTEM (high resolution transmission electron microscopy) images, which proves that they all grow along the [001]. The ultra-long AlN nanorods also exhibit the same crystalline structure and growth direction, as indicated in Fig. 4g and 4h. So it comes to a conclusion no matter what morphology these AlN nanostructures belong to, all of them are perfect single crystals with a growth orientation of [001].

Energy dispersive x-ray (EDX) characterization is performed on different morphologies of AlN nanostructures. These nanostructures have resembled EDX spectrum, so only a typical spectrum is given here. It is clear that the Al L_1, L_2 and L_3-edge peaks (corresponding to its inner energy levels) are existed in Fig. 5a. From the inset, the characteristic peak of N k-edge can be also found in the spectrum. Moreover, Gatan EELS analysis also shows that the total content of element Al and N is over 98 %, thus it can be confirmed that these nanostructures are pure AlN single crystals whether they are in any morphology.

To further comprehend the effect of the experimental parameters to the morphology of AlN nanostructures and understand the growth mechanism for different nanostructures, the detailed synthesis conditions are provided in Table 1. As for the growth of AlN nanocone, nanorod and nanocrater, Fe_3O_4 nanoparticles are used as the catalyst. So we preferred the vapor-liquid-solid (VLS) mechanism to illustrate the formation of AlN nanostructures. Because not any catalysts are found to exist at the top of these three nanostructures, it is proposed that the growth model of these nanostructures is the bottom growth model. As explained in the reference, the tight bonding force may exist between the catalyst and the substrate at the beginning of the growth (Fan et al., 1999). The formation mechanism of three morphologies of AlN nanostructures may be attributed to the diffusion mediated growth mechanism (Shi et al., 2005). Based on this model (Shi et al., 2005), AlN precursors have different diffuse length for different growth planes, and these growth planes should have different growth rate at different temperature at the same time. The anisotropy of the growth plane at different temperature will lead to the formation of nanorod or nanocone, i.e., high temperature (>900 ◦C) benefits for the synthesis of AlN nanorods, as shown in Table 1.

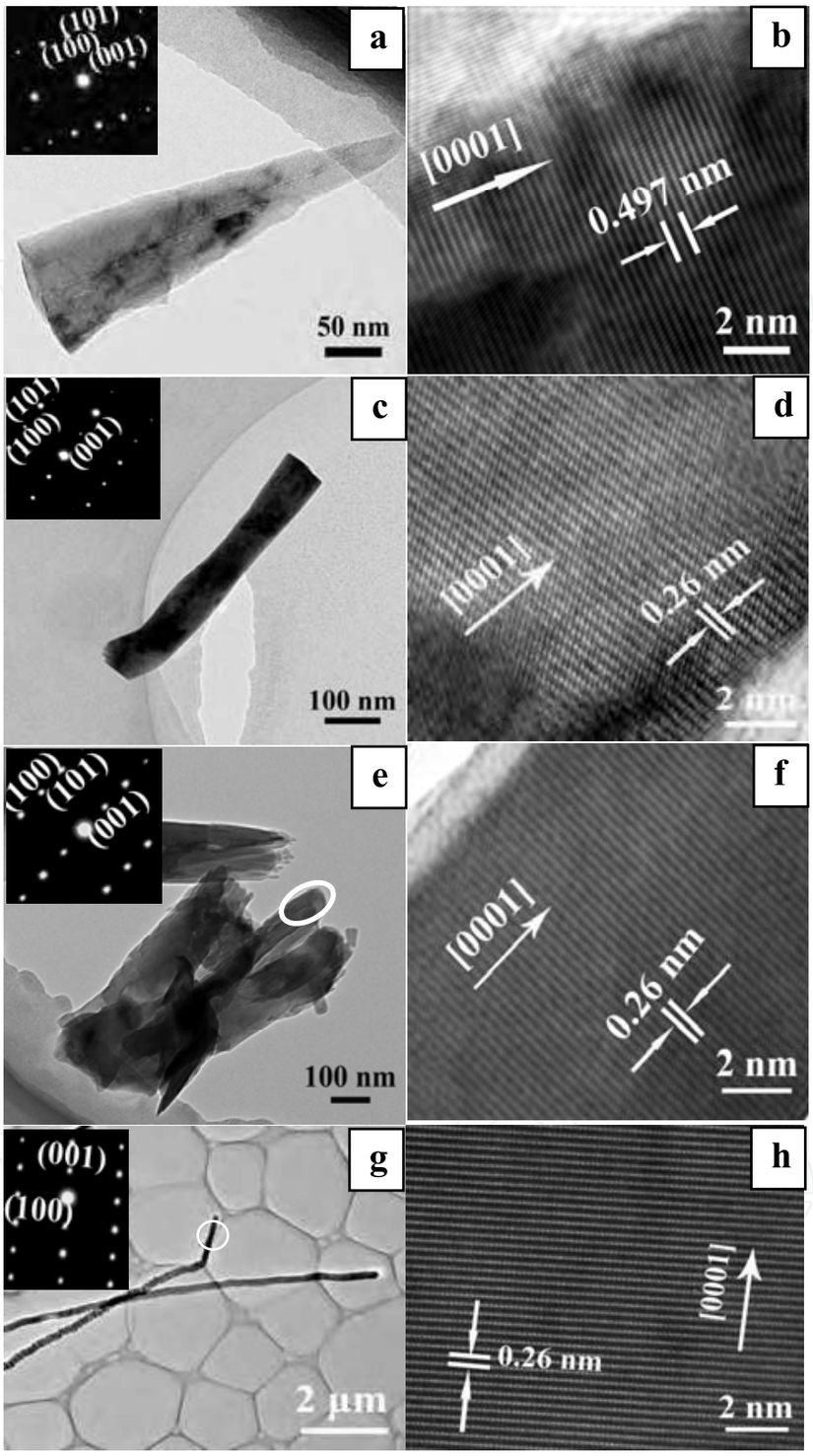

Fig. 4. Typical TEM and HRTEM images of four kinds of AlN nanostructures (a, b) AlN nanocones; (c, d) AlN nanorods; (e, f) AlN nanocraters. (g, h) ultra-long AlN nanorods. The inset is their corresponding SAED pattern and the white circle in Fig. 4e and 4g respectively corresponds to the region in the HRTEM image of Fig. 4f and 4h.

Experimental conditions / Sample	Source material ratio (Al : Fe_2O_3)	Carrier gas	Growth temperature (^oC)	Length (μm)	Outer diameter (nm)	Growth density (/cm^2)
Nanocone	0.2 g: 0 g	N_2, NH_3	700-800	2	40	$2.2x10^9$
Nanorod	0.2 g: 0 g	N_2, NH_3	900-1000	2	150	$1.5 x10^9$
Nanocrater	0.2 g: 0 g	N_2, NH_3	800-900	2	400	$3 x10^8$
Ultra-long nanorod	0.6 g : 0.2 g	N_2, NH_3, H_2	1000-1200	50	100	$3.2x10^7$

Table 1. The list of morphological characteristics and experimental conditions for different morphologies of AlN nanostructures.

When slightly increasing the growth temperature (still lower than the temperature of the nanorod) at the same molecular ratio of the reaction gas (NH_3/N_2) of the nanocone, the AlN nanocraters can be synthesized. More AlN vapors can dissolve in the catalyst solutions at the growth stage of nanocrater than the formation of AlN nanocones at this situation. Subsequently more AlN seeds can separate from oversaturated solutions because of the overmuch supplement of the vapors in the following stage. Because the concentration of the catalyst is too high, the density of the catalyst becomes too high and the distance between the catalysts turns short accordingly. At the driving of high temperature, the neighbor catalysts migrate to gather together to form larger precursors for the new seeds in synthesizing new nanostructures, which should be the most energy favorable structures. Finally, the nanocraters are fabricated from these gathered precursors with the progress of the reaction.

Although the VLS mechanism may be used to illustrate the formation of the nanocone, nanorod and nanocrater, it is not suitable for the ultra-long nanorods because no catalyst is used in their synthesis process. So the self-catalyzing Vapor-Liquid-Solid (VLS) mechanism (Liu et al., 2004; Z. L. Wang et al., 2003) is proposed to explain the growth of ultra-long AlN nanorod. At the initial stage, the Al powders were evaporated to Al atoms at melting point of about 650 ^oC and transferred to the region of the substrate by the carrier gas. Subsequently, the transportation Al atoms deposited on the substrate with lower temperature and formed a continuous Al film. At the function of H_2 gas, the continuous film gradually separated into Al nanoparticle film, as described in Ref. (Yao et al., 2008; Jung et al., 2001.) When the temperature was increased to 1000 ^oC, NH_3 gas was introduced into the vacuum chamber and decomposed into N atoms. At high temperature (>1000 ^oC), Al nanoparticle precursors turned liquid droplets on the substrate. So the foreign N atoms reacted with the Al liquid droplets and formed the AlN precursors as the seeds of the ultra-long nanorod in the solutions. AlN seeds can continuously separate from oversaturated solutions because of the overmuch supplement of AlN precursors. Finally, with the progress of the reaction, high density of ultra-long AlN nanorod arrays was synthesized on the substrate. And the steric overcrowding (Liu et al., 2004, 2005, 2008; Cao et al., 2003) for these nanostructures is considered as the possible aligned mechanism of AlN nanostructure arrays.

As summarized in Table 1, the growth conditions will influence their density. Through a series of designed experiments, it is found that the growth temperature is the determinate factor for the formation of different morphology of AlN nanostructures. Moreover, the total mass of the source materials has effect on the growth density of the nanostructures. It is observed that the lower mass of raw materials will induce lower density of nanostructure. It

is also seen that the ultra-long Al nanorod is hard to be synthesized when the mass ratio of Al powders to Fe_2O_3 powders is lower than 8:1. In addition, the pressure of the carrier gas also takes effects on the synthesis of these nanostructures. If the growth pressure is adjusted to be lower than 100 Pa, only AlN thin film can be found on the substrate.

The surface electron affinity is one of important parameters determining the field emission property of cathode nanomaterials. It is known that AlN nanostructures may have a little positive or negative affinity on (001) crystalline plane, which make them as one of the promising cathode materials in future. The Ultraviolet Photoemission Spectroscopy (UPS) technique is applied to measure the electron affinity of the AlN nanostructures before the beginning of FE measurements. Because these nanostructures have similar UPS spectrum, only a representative spectrum of the sample is given in Fig. 5b. To confirm that the detector can collect all emission electrons from the valence band, a negative 5 voltage was applied to the sample. The whole spectral width ($W_{spectra}$) of the sample can be calculated by linearly extrapolating the emission onset edges to zero intensity at both the low kinetic energy cutoff and the high kinetic end, which are equal to the energy difference between the deepest level in the valence band and the edge of the valence band for semiconductor. According to this method, its width is determined to be about 14.3 eV. The surface electron affinity χ of a sample may be obtained using the equation given below (Benjamin et al., 1996):

$$\chi = h\nu - E_g - W_{spectra} \tag{1}$$

where E_g is the energy band gap, and hν=21.2 eV, which is the radiation energy of He I line. The energy band gap of AlN nanostructures can be assumed to be the same as that of bulk AlN, i.e., 6.28 eV (Edgar et al., 1999). Then the χ values are deduced to be 0.62 eV, which suggests the electron affinity of the as-prepared AlN nanostructures is low enough for electron emission at low voltage operations in FE area.

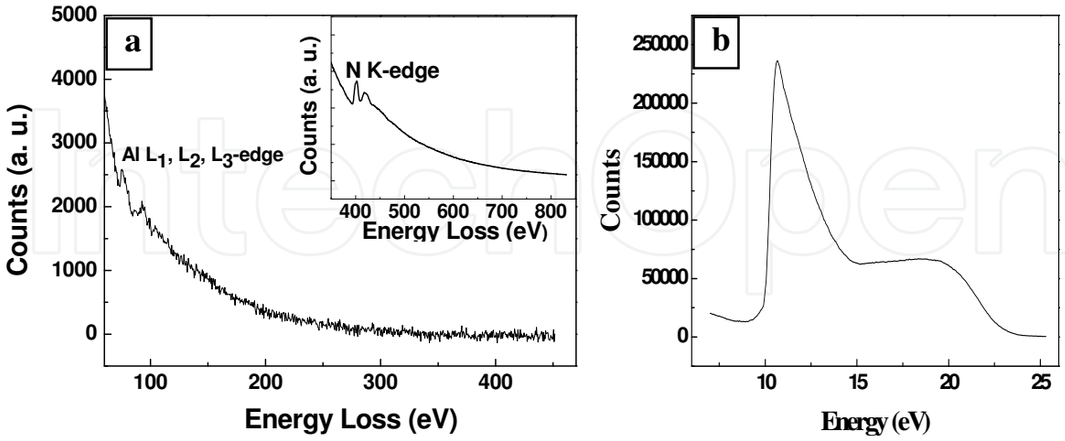

Fig. 5. (a) Representative EELS spectrum of the AlN nanostructures. (b) Their UPS spectrum.

Whether these synthesized AlN nanostructures are promising cold cathode nanomaterials needs to be further valued by their FE properties. Their field emission measurements are carried out in the field emission analysis system, whose base pressure is lower than $3x10^{-7}$

Pa. Transparent anode method was used in the measurements to obtain the FE behaviors of the total film in different morphology. These three samples were applied as the cathodes and the indium-tin-oxide (ITO) glass was used as anode. The area of the samples was around 1x1 cm² and the measurement distance between the anode and the cathode is about 400 μm. The J-E curves and FN plots of the nanocones, the nanorods, the nanocraters and the ultra-long nanorods are shown in Fig. 6a and 6b, respectively. By comparing their FE

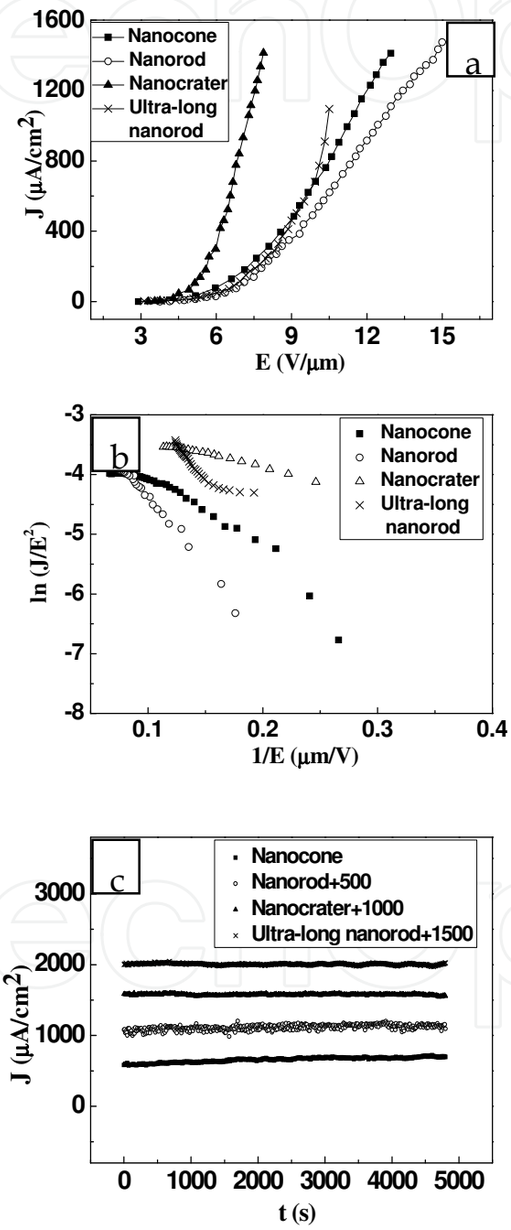

Fig. 6. (a) The field current density-electric field (J-E) curves of the AlN nanostructures in different morphology; (b) Their corresponding FN plots. (c) The stability curves of the AlN nanostructures in different morphology in field emission process.

behaviors, it is clear that the AlN nanocraters have the best FE performance with a turn-on field (defined as the field at 10 μA/cm²) of 3.9 V/μm and a threshold field (defined as the field at 1 mA/cm²) of 7.2 V/μm. It is also found that the FE properties of the AlN nanorods are better, those of the nanocone are worse, and those of the ultra-long AlN nanorods are the worst among them, as provided in Table 2. But even for the AlN ultra-long nanorods with the worst FE performance, their FE behaviors are comparable with many cathode nanomaterials, such as ZnO, WO_3 and CuO. In addition, all of their FN plot exhibits a nonlinearity relationship within the range.

What leads to their different FE performance for different nanostructures is an important question, which is intensively related with their applications. We proposed the following interpretations to analyze the possible mechanism. According to the Metal-Insulator-Vacuum (MIV) theory (Latham & Xu, 1995), the microscopic field E_{Local} acting at the tip of microtrusion is proportional to the enhancement factor β, which is given by

$$E_{Local} = \beta E = \beta \frac{V}{d} \tag{2}$$

In this expression, V is the applied voltage, d is the distance between the anode and the cathode, and E is the applied macroscopic field. And the enhancement factor β can be expressed as (Fursey & Vorontsov-vel'yaminov, 1967)

$$\beta = \frac{\left(\lambda^2 - 1\right)^{1.5}}{\lambda \ln\left[\lambda + \left(\lambda^2 - 1\right)^{\frac{1}{2}}\right] - \left(\lambda^2 - 1\right)^{\frac{1}{2}}} \tag{3}$$

where $\lambda = l / r$ is the aspect ratio, i.e., the length of the nanostructure versus its top radius. As discussed in the above theory, the nanostructure with the large aspect ratio should have high β value because they have more strong ability of amplification macroscopic field than other nanostructures at the same applied field. So the nanorod, the nanocones and the nanocraters should have better FE behaviors than the ultra-long nanorods according to this theory. But as observed in Table 2, the FE properties of the ultra-long nanorod with the highest aspect ratio (500) are worse than those of the nanocrater with lower aspect ratio (50), which suggests that this theory can't be directly used to explain the phenomena.

Then at this situation, another discrepancy existed in these nanostructures must be considered due to the screen effects (Bonard et al., 2001; Wang & Tong, 1996), which is their growth density. According to this theory, the surface of the nanostructured film will be very close to a plane when the growth density of the nanostructure is very high. So when the field is applied between the anode and the cathode, it will prevent the macroscopic electrical field from penetrating into the nanostructures film (Bonard et al., 2001), which in versus lowers the local field amplification existing among the nanostructures and make electron emission hard to occur. Based on the classical Fowler-Nordheim (FN) theory (Fowler & Nordheim, 1928), the relationship between current density J and applied field E should be described as follows:

$$J = \eta a \left(\frac{\beta^2 E^2}{\varphi} \right) \exp\left(\frac{-B\varphi^{\frac{3}{2}}}{\beta E} \right), \tag{4}$$

Where a=1.54x10^{-6} (AV^{-2}eV), B=6.83x10^{9} (Vm^{-1}eV^{-3}/2), and φ is the work function of the cathode emitters, which adopts 3.7 eV for AlN (Edgar et al., 1999). So the enhancement

FE Properties / Morphology	Aspect ratio	Turn-on field at 10 μA (V/μm)	Threshold field at 1 mA (V/μm)	β	s (field screen parameter)	Emission Instability (2 h)
Nanocone	50	4.2	11.3	1740	0.087	9 %
Nanorod	23	4.9	12.4	1250	0.234	7 %
Nanocrater	50	3.9	7.2	2140	0.2675	4 %
Ultra-long Nanorod	500	4.5	10.4	1997	0.250	6 %

Table 2 The list of comparisons on the field emission parameters of the as-prepared AlN nanostructures in different morphology.

factor β values of the AlN nanostructures can be calculated from the slopes of their FN plots, which reflect the amplification ability of macroscopic field. From Table 2, it is observed that the obtained β values are ranging from 1250 to 2140, which suggests that AlN nanostructures are one of the most promising FE materials in future. It can be observed in Table 2 that the nanorod and the nanocrater with lower density have higher field enhancement factor β than the nanocones with higher density. Combined the nonlinearly (low and high electric field)exhibited in their FN plots with the screen effect, Filip model was more appropriate for these samples (Filip et al., 2001), which can be expressed as follows:

$$E_{local} = s\frac{V}{r} + (1-s)\frac{V}{d}, \tag{5}$$

Where E_{local} is the local field nearby the emitters when considering the screen effect, r is the radium of the tip of the emitter, s is the screen effect parameter, V is the applied voltage and d is the distance between the anode and cathode, which is 400 μm in our measurements. Combined equation (2) with (5) and considered the d/r value is far higher than 1 in our experiment, the field enhancement factor can be derived as:

$$\beta \approx 1 + s\frac{d}{r} \Rightarrow s = \frac{(\beta - 1)r}{d}, \tag{6}$$

Substitute typical d value, r value and β value obtained for four samples, their corresponding field effect parameter s can be obtained, which is indicated in Table 2. It is clear that the smaller the s value, and the greater the role that screening effect plays in the actual field emission process. So it is concluded that the field screen effect of the nanocone is the most distinguished among these four nanostructures because of its smallest s value (0.087). Therefore, the nanocraters should have the best FE behaviors and the nanorods should have better FE behaviors among these four nanostructures based on this rule, which

is in well agreement with our observed results in Fig. 6. Moreover, the nonlinearity of the FN plots of four samples can also be explained by Filip model (Filip et al., 2001). It is also proposed that the morphology and the growth density of the AlN nanostructures determine their FE behaviors to a great extent.

The emission stability of nanostructures is another question need to be paid much attention for their actual application in FE area, and Fig. 6c shows the stability curves of the AlN nanostructures in different morphology. Because the stability appearance at high working current is more important than at low current for application, the emission current was kept at 500 μA at the beginning of the measurement whether they are in what morphology. The whole measurement lasted for 2 hours. It is seen in Fig. 6c that the nanocraters are found to possess the most stable emission performance with a current fluctuation lower than 4 % and the nanocones are the worst (9 %), as indicated in Table 2. Other nanostructures also exhibit excellent field emission stability, which is good enough for the potential application in field emission area. In combined with all the field emission behaviors of these four AlN nanostructures, we can draw a conclusion that the AlN nanocrater arrays have the best FE performance whether from the turn-on field or the stability, which should have the most promising future in FE applications.

Then, what to do for further inproving their field emission properties? We should firstly find the important factor, which strongly affects their emission performance. In order to confirm this, measurement on individual AlN ultra-long nanorod is very essential because many physical information of AlN nanostructure is concealed by the continuous film due to some effects. Few reports so far are concerned with the characterization of individual single AlN ultra-long nanorods because the AlN nanostructures are often fabricated in high density, which is hard to carry out the in-situ measurement on the physical properties of individual nanostructures. Since we have mastered the controlled growth tecnique of the AlN ultra-long nanorod in growth density, measurement on the physical properties of individual nanostructure becomes feasible. The measurement was carried out in a modified SEM system, which has been depicted in detail in our previous papers (Liu et al., 2008, 2010a, 2010b; She et al., 2007). Figs. 7a and 7b provides the SEM image of the measurement during the electric conductivity process and during field emission process, respectively. It is seen from Fig. 7a that the W probe tightly contacts to individual ultra-long AlN nanorod on its end. Individual ultra-long nanorod has a length of about 50 μm and a diameter of about 100 nm, which is consistent with the observed images in Fig. 2. One can see in Fig. 7b that the distance between the W probe and individual nanorod was kept at about 2 μm through field emission measurement.

Representative curve of the electrical transportation property of individual ultra-long AlN nanorod is shown in Fig. 8a. Here only a typical I-V curve of a single nanostructure is given because their electrical conductivity is similar, having the same order (in the range from 2 x 10^{-4} – 7 x 10^{-4} $\Omega^{-1}cm^{-1}$). From the shape of the I-V curve of Fig. 8a, it can be concluded that the electric contact in conductivity measurement should be Schottky barrier rather than the ohmic contact because it is nonlinear and asymmetrical. We use the following descriptions to illutrate this phenomena. The contact resistance $R_{Contact}$ in measurements can be divided into two types, in which one is the contact resistance R_1 between the nanorod and the substrate and another is the contact resistance R_2 between the nanorod and the W probe, which can be written as:

$$R_{Contact} = R_1 + R_2 \tag{7}$$

So the total resistance R_{Total} consists of the contact resistance $R_{Contact}$ and the intrinsic resistance R_{AlN} of AlN nanorod, which is as follows:

$$. R_{Total} = R_{AlN} + R_{Contact} = R_{AlN} + R_1 + R_2 \tag{8}$$

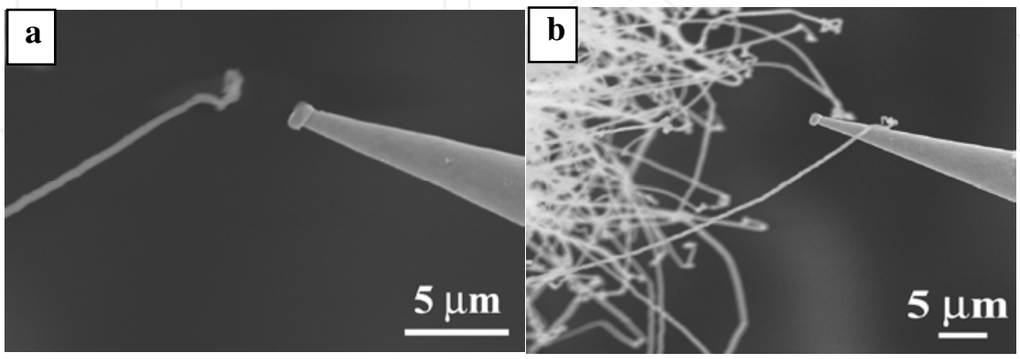

Fig. 7. The SEM images of individual AlN nanorod and the tungsten probe (a) during the conductivity measurement, and (b) during the field emission measurement.

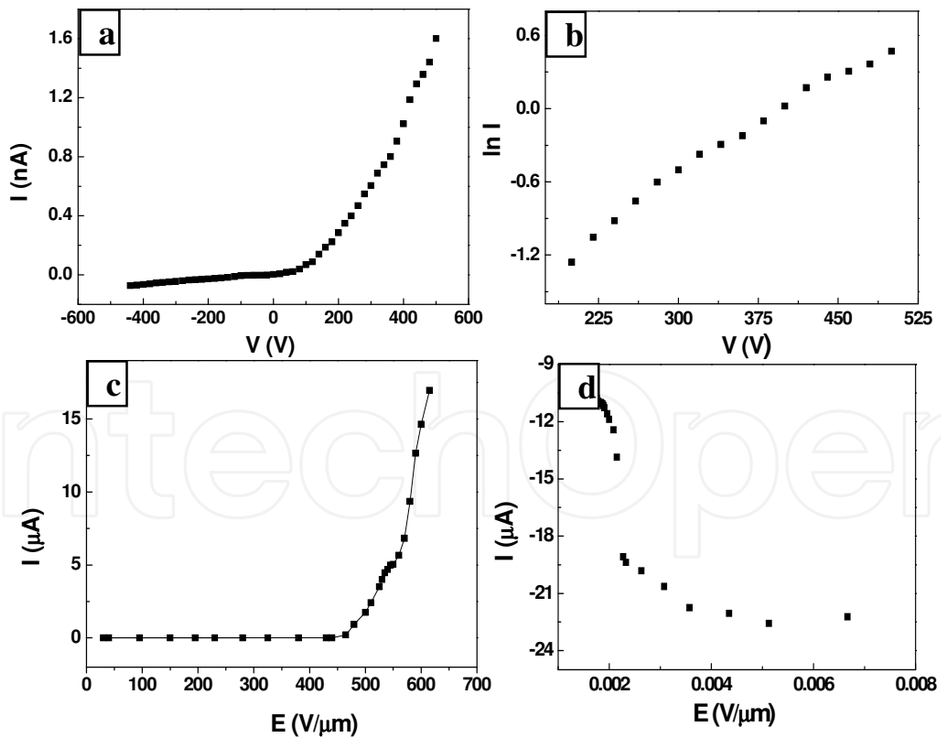

Fig. 8. (a) Representative electrical transport curve of single AlN nanorod. (b) The lnI versus V curve in conductivity measurment. (c) The field emission I-E curves of single nanorod. (d) Its corresponding FN plots.

The work function of W, AlN and n-doped Si is usually 4.5 eV, 3.8 eV and 4.2 eV, respectively. At high growth-temperature over 1100 ^{o}C, the AlN clusters and n-doped Si will be alloyed together, which suggests that their contact resistance R_1 is very low close to ohmic contact after the growth. But for R_2, high contact resistance will occur because their large discrepancy of the work function between W probe and individual AlN nanorod, which results in the formation of Schottky barrier. In this situation, R_2 determines the contact resistance $R_{Contact}$. Based on the thermionic emission theory (Heo et al., 2004; Sze et al., 1971), the reverse current of an ideal Schottky barrier should be at a very low level because the barrier is often elevated to a very high value at reverse voltage, so the reverse current can be neligible in contrast to their positive current. The positive current will exponentially increase with the positive voltage applied on the Schottky diode, followed by the equation (Sze et al., 1971)

$$J(V,\varphi_b) = A^* T^2 \exp\left(-\frac{\varphi_b}{kT}\right)\exp\left(\frac{qV}{nkT}\right)\times\left[1-\exp\left(-\frac{qV}{kT}\right)\right] \tag{9}$$

, where $A^*=4\pi m^* qk^2/h^3$ is the Richardson constant of the semiconductor, φ_b is the effective height of Schottky barrier, k is the Boltzmann constant, q is the magnitude of electron charge, n is usually adopted to be 1 for ideal Schottky diode, T is the absolute temperature. According to this equation, the linear behavior of lnI versus V should be observed at positive voltage. It is clearly seen in Fig. 8b that lnI has a linear relation with V, which is in well agreement with the proposed theoretical results. It suggests that the electron transportation process of measurement on individual nanorod should obey the thermionic emission model, which proves our explaination on Schottky barrier is reasonable. Moreover, the electrical conductivity can be obtained by approximately calculating the slope of I-V curve at high voltage. It can be understood that the intrinsic resistance R_{AlN} dominates the total resistance R_{Total} because the Schottky barrier at positive voltage will rapidly decreased to a very low value with the the increasing of the applied voltage, which is far lower than R_{AlN}. So based on this way, the intrinsic conductivity of AlN nanorod is deduced to be 2.7×10^{-4} $\Omega^{-1}cm^{-1}$, which is almost 10^2 times larger than with that (8×10^{-6} $\Omega^{-1}cm^{-1}$) of other researcher group (Zheng et al., 2008). The relatively higher conductivity should be originated from the doping of element Si and Fe, which incorporated into the engergy gap of AlN to be a shallow impuries energy level. Element Si may come from the Si substrate or quartz tube, and element Fe may come from Fe_2O_3 in source powders, which possibly diffused into AlN nanorods during the high-temperature growth process. Therefore, the intrinsic electric conductivity of ultra-long AlN nanorod is overestimated in this measurement.

Fig. 8c gives typical field emission current versus applied field (J-E) curve of a single ultra-long AlN nanorod, and its corresponding Fowler-Nordheim (FN) plot is indicated in Fig. 8d. From Fig. 8d, individual AlN nanorod is observed to have a mean 1 nA field (defined as the electric field when the emission current is 1 nA) of 440 V/μm and 1 μA field (defined as the electric field when the emission current is 1 μA) of 480 V/μm. The FE performance of the as-synthesized ultra-long AlN nanorod is better than that of AlN nanocones (500 nA at 1000 V//μm) in recent report (Bonald et al., 2001), which should come from the conductivity of individual nanorod on our synthesis process is higher than that in other researher groups due to the doping of element Fe and Si. It is also found that the field emission current exhibits a increase tendency with the applied field and doesn't reach the saturation until the

applied field arrives at 800 V/μm, which proposes AlN nanorod has a high endurance ability to large emission current due to its high thermal conductivity. The FN plots of individual AlN nanorod is seen to be nonlinear. We attributed the nonlinear behavior of the FN plots to be the drecrease of the contact resistance R_2 with the increase of the temperature followed by high applied field, because of which induces higher effective field appearing between cathode and anode. Even though it is found from Fig. 8c that the FE property of individual AlN nanorod is not very good, in comparison with the others such as boron nanotubes and nanowires (Liu et al., 2008, 2010a, 2010b), $W_{18}O_{49}$ (Li et al., 2009) etc, as we reported early, and that this finding is in consistent with the findings reported above for the FE performance of AlN nanorod films. The relatively worse FE performance of a single AlN nanorod is strongly related to its low intrinsic electrical conductivity, as may be explained in the following. It is obvious that the intrinsic conductivity of individual AlN nanorod in our experiment is lower than that of many nanomaterials with excellent FE properties, such as CNTs (1 - 2 x 10^3 $\Omega^{-1}cm^{-1}$) (Dai et al., 1996), $W_{18}O_{49}$ nanorod (10^{-1} - 10^{-2} $\Omega^{-1}cm^{-1}$) (Li et al., 2009), ZnO (2 - 4 x 10^{-2} $\Omega^{-1}cm^{-1}$) (She et al., 2008) and boron nanotube (10 - 20 $\Omega^{-1}cm^{-1}$) (Liu et al., 2010). So when an equal voltage is applied, more voltage drops on the nanorod's intrinsic reistance rather than falls across the vacuum gap between nanorod and anode probe, which leads to a lower effective field at the tip of the nanorod. Thus, relatively higher turn-on and threshold field is needed for the AlN nanorod in order to realize the tunnel effects, which results in their not very good FE performance. The relatively worse FE properties of individual nanorod must naturally take effect on the emission performance of their corresponding film. It is known that the element-doping can effectively improve the electric conductivity of individual nanostructures by forming a impurities energy level in their energy gap, which can provide enough electrons for tunnel current at low applied field. Once the electric conductivity of AlN nanostructures can be enhanced to a high level, they should have a more promising future in FE devices.

4. Conclusions

Different morphology of AlN nanostructure arrays have been successfully synthesized by CVD technique. They are confirmed to have perfect single crystalline AlN structures with a growth direction of [001]. The VLS and Self-catalyzing VLS mechanism is respectively used to explain the formation mechanism for these four nanostructures. And the AlN nanocrater arrays are found to have the best FE properties among four kinds of nanostructures, which have a turn-on field of 3.9 V/μm and a threshold field of 7.2 V/μm. Moreover, measurements on individual ultra-long nanorods show that they have a lower electric conductivity (2.7 x 10^{-4} $\Omega^{-1}cm^{-1}$) and relative worse FE performance (1 nA field of 440 V/μm and 1 μA field of 480 V/μm) than CNTs. The former leads to their FE performance. All of the synthesized AlN nanostructure arrays exhibit good FE performance, which suggests that they should be one of the most promising cold cathode nanomaterials in future.

5. Acknowledgements

The authors are thankful for the support from the National Basic Research Program of China (973 Program, Grant No. 2007CB935501, 2010CB327703, Grant No. 50802117, 51072237, 50725206,), the National Joint Science Fund with Guangdong Province (Grant No. U0634002, U0734003), the Foundation of Education Ministry of China (Grant No. 20070558063 and

2009-30000-3161452), the Science and Technology Department of Guangdong Province, the Education Department of Guangdong Province, and the Science and Technology Department of Guangzhou City.

6. References

Benjamin, M. C.; Bremser, M. D.; Jr., T. W. Weeks., King, S. W.; Davis, R. F.; Nemanich, R. J. (1996). UV Photoemission Study of Heteroepitaxial AlGaN Films Grown on 6H-SiC, *Appl. Surf. Sci.*, Vol. 104/105, No. , (September 1996) , pp. 455-460, ISBN 0169-4332

Bonard, J. M.; Weiss, N.; Kind, H.; Stöckli, T.; Forró, L.; Kern, K.; Châtelain, A. (2001). Tuning the Field Emission Properties of Patterned Carbon Nanotube Films, *Adv. Mater.*, Vol. 13, No. 3, (February 2001), pp. 184-188, ISBN. 0935-9648

Cao, P. J.; Gu, Y. S.; Liu, H. W.; Shen, F.; Wang, Y. G.; Zhang, Q. F.; Wu, J. L.; Gao, H. J. (2003). High-Density Aligned Carbon Nanotubes with Uniform Diameters, *J. Mater. Res.*, Vol. 18, No. 7, (July 2003), pp. 1686-1690, ISBN 0022-2402

Davis, R. F., (1991). III-V Nitrides for Electronic and Optoelectronic Applications, *Proceeding of the IEEE.*, Vol. 79, No. 5, (May 1991), pp. 702-712, ISBN 0018-9219

Dai, H.; Wong, E. W.; Lieber, C. M. (1996). Probing Electrical Transportation Properties in Nanomaterials: Conductivity of Individual Carbon Nanotubes, *Science*, Vol. 272, No. 5261, (April 1996), pp 523-526, ISBN 0036-8075

Edgar, J. H., Strite, S.; Akasaki, I.; Amano, H.; Wetzel, C. (1999). Properties, Processing and Applications of Gallium Nitride and Related Semiconductors, INSPEC., ISBN 978-0-86341-775-7, Part A, London, UK

Fan, S. S.; Chapline, M. G.; Franklin, N. R., Tombler, T. W.; Cassell, A. M. ; Dai, H. J. (1999). Self-Oriented Regular Arrays of Carbon Nanotubes and Their Field Emission Properties, *Science*, Vol. 283, No. 5401, (January 1999), pp. 512-514, ISBN 0036-8075

Fan, Z. Y.; Wang, D. W.; Chang, P. C.; Tseng, W. Y.; Lu, J. G. (2004). ZnO nanowire Field-Effect Transistor and Oxygen Sensing Property, *Appl. Phys. Lett.*, Vol. 85, No. 24, (December 2004), pp. 5923-5925, ISBN 0003-6951

Filip, V.; Nicolaescu, D.; Tanemura, M.; Okuyama, F. (2001). Modeling the Electron Field Emission from Carbon Nanotube Films, *Ultramicroscopy*, Vol. 89, No. 1-3, (October 2001), pp. 39-49, ISBN 0304-3991

Fowler, R. H. & Nordheim, L. W. (1928). Electron Emission in Intense Electric Fields, *Proceeding of the Royal Society of London*, Ser. A, Vol. 119, No. 781, (May 1928), pp. 173-181

Fursey, G. N. & Vorontsov-Vel'yaminov, P. N. (1967). Qualitative Model of Initiation of Vacuum Arc II. Field Emission Mechanism of Vacuum Arc Onset, Sov. Phys: Tech. Phys., Vol. 12, No. 5, (May 1967), pp. 1377-1385, ISBN 0038-5662

Geis, M. W.; Efremov, N. N.; Woodhouse, J. D.; McAleese, M. D.; Marchywka, M.; Socker, D. G.; Hochedez, J. F. (1991). Diamond Cold Cathode, *IEEE Electron Device Lett.*, Vol. 12, No. 8, (August 1991), pp. 456-459, ISBN 0741-3106

He, S. T.; Yao, J. N.; Jiang, P.; Shi, D. X.; Zhang, H. X.; Xie, S. S.; Pang, S. J.; Gao, H. J. (2001). Formation of Silver Nanoparticles and Self-Assembled Two-Dimensional Ordered Superlattice, *Langmuir*, Vol. 17, No. 5, (February 2001), pp. 1571-1575, ISBN 0743-7643

Jung, M.; Eun, K. Y.; Lee, J. K.; Baik, Y. J.; Lee, K. R.; Park, J. W. (2001). Growth of Carbon Nanotubes by Chemical Vapor Deposition, *Diamond Relat. Mater.*, Vol. 10, No. 3-7, (March 2001), pp 1235-1240, ISBN 0925-9635

Kang, D.; Zhirnov, V. V.; Sanwald, R. C.; Hren, J. J.; Cuomo, J. J. (2001). Field Emission from Ultrathin Coatings of AlN on Mo Emitters, *J. Vac. Sci. Technol. B*, Vol. 19, No. 1, (January 2001), pp. 50-54, ISBN 1071-1023

Latham, R. V. & Xu, N. S. (1995). High Voltage Vacuum Insulation, Academic, ISBN 0-12-437175-2 , London, UK

Li, Z. L.; Liu, F.; Xu, N. S. (2009). Improving field-emission uniformity of large-area $W_{18}O_{49}$ nanowire films by electrical treatment, J. Vac. Sci & Technol. B, Vol. 27, No. 6, (December 2009), pp. 2420-2425, ISBN 1071-1023

Liu, C.; Hu, Z.; Wu, Q.; Wang, X. Z.; Chen, Y.; Sang, H.; Zhu, J. M.; Deng, S. Z.; Xu, N. S. (2004). Vapor−Solid Growth and Characterization of Aluminum Nitride Nanocones, *J. Am. Chem. Soc.*, Vol. 127, No. 4, (January 2004), pp. 1318-1322, ISBN 0002-7863

Liu, F.; Cao, P. J.; Zhang, H. R.; Li, J. Q.; Gao, H. J. (2004). Controlled Self-Assembled Nanoaeroplanes, Nanoflowers and Tetrapod Networks of Zinc Oxide, *Nanotechnology*, Vol. 15, No. 8, (August 2004), pp. 949-952, ISBN 0957-4484

Liu, F.; Cao, P. J.; Zhang, H. R.; Shen, C. M.; Wang, Z.; Li, J. Q.; Gao, H. J. (2005). Well Aligned ZnO Nanorods and Nanorods Prepared Without Catalysts, *J. Cryst. Growth*, Vol. 274, No 1-2. , (January 2005), pp. 126-131, ISBN 0022-0248

Liu, F.; Tian, J. F.; Bao, L. H.; Yang,T. Z.; Shen, C. M., Lai, X. Y.; Xiao, Z. M.; Xie, W. G.; Deng, S. Z.; Chen, J.; She, J. C.; Xu, N. S.; Gao, H. J. (2008). Fabrication of Vertically Aligned Single Crystalline Boron Nanowire Arrays and Investigation on Their Field Emission Behaviors, *Adv. Mater.*, Vol. 20, No. 13, (July 2008), pp. 2609-2615, ISBN 0935-9648

Liu, F.; Su, Z. J.; Liang, W. J.; Mo, F. Y.; Li, L.; Deng, S. Z.; Chen, J.; Xu, N. S. (2009). Controlled Growth and Field Emission Investigation of Vertically Aligned AlN Nanostructures in Different Morphology, *Chin. Phys. B*, Vol. 5, No. 18, (May 2009), pp. 2016, ISBN 1674-1056

Liu, F. ; Su, Z. J.; Li, L; Mo, F. Y.; Jin, S. Y.; Deng, S. Z.; Chen, J; Shen, C. M.; Gao, H. J.; Xu, N. S. (2010). Effect of Contact Mode on the Electrical Transport and Field Emission Performance of Individual Boron Nanowire, *Adv. Funct. Mater.*, Vol. 20, No. 12, (June 2010), pp. 1994-2003, ISBN 1616-301X

Liu, F.; Shen C. M.; Su, Z. J.; Ding, X. L.; Deng, S. Z; Chen, J; Xu, N. S.; Gao, H. J. (2010). Metal-like Single Crystalline Boron Nanotubes and Their Electric Transport and Field Emission Properties, *J. Mater. Chem.* , Vol. 20, No. 11, (January 2010), pp. 2197-2205, ISBN 0022-2461

Nicolaescu, I. V.; Tardos, G.; Riman, R. E. (2005). Thermogravimetric Determination of Carbon, Nitrogen, and Oxygen in Aluminum Nitride, J. Am. Ceram. Soc., Vol. 77, No. 9, (March 2005), pp. 2265-2272, ISBN 0002-7820

Paul, R. K.; Lee, K. H.; Lee, B. T.; Song, H. Y. (2008). Formation of AlN Nanowires Using Al Powder, *Mater. Chem. Phys.*, Vol. 112, No. 2, (December 2008), pp. 562-565, ISBN 0254-0584

Ponthieu, E.; Grange, P.; Delmon, B.; Lonnoy, L.; Leclercq, L.; Bechara, R.; Grimblot, J. (1991). Proposal of A Composition Model for Commercial AlN Powders, *J. Eur. Ceram. Soc.*, Vol. 8, No. 4, (April 1991), pp. 233-241, ISBN 0955-2219

She, J. C.; An, S.; Deng, S. Z.; Chen, J.; Xiao, Z. M.; Zhou, J.; Xu, N. S. (2007). Laser Welding a Single Tungsten Oxide Nanotip on a Handable Tungsten Wire: A Demonstration of Laser-welding Nanoassembly, *Appl. Phys. Lett.*, Vol. 90, No. 7, (February 2007), pp. 073103-1-3, ISBN0003-6951

She, J. C.; Xiao. Z. M.; Yang, Y. H.; Deng, S. Z.; Chen, J.; Yang, G. W.; Xu, N. S (2008). Correlation Between Resistance and Field Emission Performance of Individual ZnO One-dimensional Nanostructures, *ACS Nano*, Vol. 2, No. 10, (September 2008), pp. 2015-2022, ISBN 1936-0851

Sheppard, L. M. (1990). Aluminum Nitride: A Versatile but Challenging Material, *Am. Ceram. Soc. Bull.*, Vol. 69, No. 11, (June 1990), pp. 1801-1812, ISBN 0002-7812

Shi, S. C.; Chen, C. F.; Chattopadhyay, S.; Lan, Z. H.; Chen, K. H.; Chen, L. C. (2005). Growth of Single-Crystalline Wurtzite Aluminum Nitride Nanotips with A Self-Selective Apex Angle, *Adv. Func. Mater.*, Vol. 15, No. 5, (April 2005), pp. 781-786., ISBN 1616-301X

Shi, S. C.; Chattopadhyay, S.; Chen, C. F.; Chen, K. H.; Chen, L. C. (2006). Structural Evolution of AlN Nano-Structures: Nanotips and Nanorods, *Chem. Phys. Lett.*, Vol. 418, No. 1-3, (January 2006), pp. 152-157, ISBN 0009-2614

Sze, S. M.; Coleman, D. J.; Loya, A. (1971). Current Transport in Metal-semiconductor-metal Structures, *Solid-State Electron.*, Vol. 14, No. 12, (June 1971) pp. 1209-1218, ISBN 0038-1101

Tang, Y. B.; Cong, H. T.; Chen, Z. G.; Cheng, H. M. (2005). An Array of Eiffel-Tower-Shape AlN Nanotips and Its Field Emission Properties, *Appl. Phys. Lett.*, Vol. 86, No. 23, (June 2005), pp. 233104 1-3, ISBN 0003-6951

Wang, B. P. & Tong, L. S. (1996). A Study of the Optimum Field Emitter Shape for Vacuum Electronics Applications, *Appl. Surf. Sci.*, Vol. 94/95, (May 1996), pp. 101-, ISBN 0169-4332

Wang, Z. L.; Wang, X. Y.; Zuo, J. M. (2003). Induced Growth of Asymmetric Nanocantilever Arrays on Polar Surfaces, *Phys. Rev. Lett.*, Vol. 91, No. 18, (October 2003), pp. 185502-185505, ISBN 0031-9007

Wu, Q.; Hu, Z.; Wang, X. Z.; Lu, Y. N.; Huo, K. F.; Deng, S. Z.; Xu, N. S.; Shen, B.; Zhang, R.; Chen, Y. (2003) Extended Vapor–Liquid–Solid Growth and Field Emission Properties of Aluminium Nitride Nanowires, *J. Mater. Chem.*, Vol. 13, No. 8, (June 2003), pp. 2024-2027, ISBN 0959-9428

Yang, H. T.; Shen, C. M.; Su, Y. K.; Yang, T. Z.; Gao. H. J.; Wang, Y. G. (2003). Self-Assembly and Magnetic Properties of Cobalt Nanoparticles, *Appl. Phys. Lett.*, Vol. 82, No. 26, (June 2003), pp. 4729-4731, ISBN 0003-6951

Yao, R. H.; She, J. C.; Xu, N. S.; Deng, S. Z.; Chen, J. (2008). Self-Assembly of Au-Ag Alloy Nanoparticles by Thermal Annealing, *J. Nanosci. Nanotechnol.*, Vol. 8, No. 7, (July 2008), pp. 3487-3492, ISBN 1533-4880

Zhao, Q.; Xu, J.; Xu, X. Y.; Yu, D. P. (2004). Field Emission from AlN Nanoneedle Arrays, *Appl. Phys. Lett.*, Vol. 85, No. 22, (November 2004), pp. 5331-5333, ISBN 0003-6951

Zheng, J.; Yang, Y.; Yu, B.; Song, X. B.; Li, X. G. (2008). [0001] Aluminum Nitride One-dimensional Nanostructures: Synthesis, Structure Evolution, and Electrical Properties, *Acs Nano*, Vol. 2, No. 1, (January 2008), pp. 134-142, ISBN 1936-0851

Zhirnov, V. V.; Wojak, G. J.; Choi, W. B.; Cuomo, J. J.; Hren, J. J. (1997). Wide Band Gap Materials for Field Emission Devices, *J. Vac. Sci. Technol. A*, Vol. 15, No. 3, (May 1997), pp. 1733-1738, ISBN 0734-2101

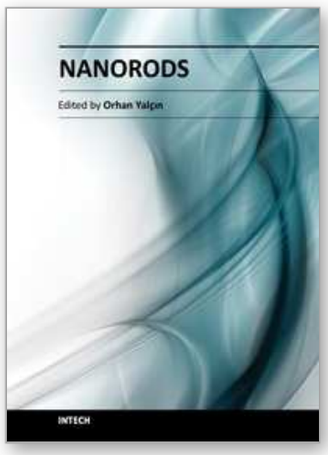

Nanorods

Edited by Dr. Orhan Yalçın

ISBN 978-953-51-0209-0

Hard cover, 250 pages

Publisher InTech

Published online 09, March, 2012

Published in print edition March, 2012

The book "Nanorods" is an overview of the fundamentals and applications of nanosciences and nanotechnologies. The methods described in this book are very powerful and have practical applications in the subjects of nanorods. The potential applications of nanorods are very attractive for bio-sensor, magneto-electronic, plasmonic state, nano-transistor, data storage media, etc. This book is of interest to both fundamental research such as the one conducted in Physics, Chemistry, Biology, Material Science, Medicine etc., and also to practicing scientists, students, researchers in applied material sciences and engineers.

How to reference

In order to correctly reference this scholarly work, feel free to copy and paste the following:

Fei Liu, Lifang Li, Zanjia Su, Shaozhi Deng, Jun Chen and Ningsheng Xu (2012). The Controlled Growth of Long AlN Nanorods and In-situ Investigation on Their Field Emission Properties, Nanorods, Dr. Orhan Yalçın (Ed.), ISBN: 978-953-51-0209-0, InTech, Available from: http://www.intechopen.com/books/nanorods/the-controlled-growth-of-long-aln-nanorods-and-in-situ-investigation-on-their-field-emission-propert

INTECH
open science | open minds

InTech Europe

University Campus STeP Ri
Slavka Krautzeka 83/A
51000 Rijeka, Croatia
Phone: +385 (51) 770 447
Fax: +385 (51) 686 166
www.intechopen.com

InTech China

Unit 405, Office Block, Hotel Equatorial Shanghai
No.65, Yan An Road (West), Shanghai, 200040, China
中国上海市延安西路65号上海国际贵都大饭店办公楼405单元
Phone: +86-21-62489820
Fax: +86-21-62489821

© 2012 The Author(s). Licensee IntechOpen. This is an open access article distributed under the terms of the Creative Commons Attribution 3.0 License, which permits unrestricted use, distribution, and reproduction in any medium, provided the original work is properly cited.

IntechOpen

IntechOpen